Facet-dependent intermediate formation and reaction mechanism of photocatalytic removing hydrophobic anthracene under simulated solar irradiation

Weixiao Qi [a], Xiaoqiang An [a,*], Fan Zhang [a,d], Huijuan Liu [b,c], Jiuhui Qu [a,c]

[a] Key Laboratory of Drinking Water Science and Technology, Research Center for Eco-Environmental Sciences, Chinese Academy of Sciences, Beijing 100085, China
[b] State Key Laboratory of Environmental Aquatic Chemistry, Research Center for Eco-Environmental Sciences, Chinese Academy of Sciences, Beijing 100085, China
[c] University of Chinese Academy of Sciences, Beijing 100049, China
[d] Hebei University of Technology, Tianjin, China

ARTICLE INFO

ABSTRACT

The intrinsic impact of inherent structures of facet photocatalysts on the reaction pathways and mechanism is largely unknown, although it is of scientific and technological importance for the research of water remediation. In this paper, hydrophobic anthracene (Ant) and TiO_2 with dominant {001}, {010} and {101} facets were selected as typical examples, to demonstrate the significant influence of exposed facets on the radical formation and intermediate production. The results showed that {101} faceted TiO_2 showed superior catalytic activity than {001} and {010} faceted TiO_2 during the degradation of Ant under simulated solar irradiation, while {001} faceted TiO_2 resulted in the largest production of anthraquione (AQ) intermediates. A fundamental study indicated that holes and oxygen played the important roles in the first step of catalytic oxidation of Ant on {001} and {010} faceted TiO_2, while •OH radical was the main species to degrade AQ. The electron spin resonance spectroscopy measurements showed that their different abilities for the in-situ formation of •OH radicals led to the differences in the intermediate products and reaction pathways. This work provides new insights into the development of high-efficiency photocatalysts for pollutant elimination through crystal-facet tailoring.

1. Introduction

Polycyclic aromatic hydrocarbons (PAHs) are a type of ubiquitously-existed pollutants in the environment [1–3]. They could derive from combustion of fossil fuels and wood, refuse burning, coke oven, pyrolysis, forest and agricultural fires [4,5]. PAHs have been largely noticed and studied due to their own potential teratogenicity, mutagenicity and carcinogenicity, and possible derivation to more toxic product, such as nitro-PAHs (NPAHs) and oxy-PAHs (OPAHs) [6–10]. Due to hydrophobic and recalcitrant properties, PAHs and their derivatives are prone to adsorbing and accumulating around the interface of particulate matters. Thus, it is of great importance to eliminate PAHs pollutants in water through heterogeneous reactions. Among various techniques, photocatalysis has become one of the most attractive methods for

water remediation. The feasibility of catalyzed degradation of PAHs over photocatalysts has been investigated [11,12]. Unfortunately, their possible industrial application is limited by the moderate removal efficiency. In order to achieve high-efficiency photocatalysis, both new material strategy and fundamental understanding of the degradation mechanism are highly desirable.

Recently, tremendous efforts have been made to improve photocatalytic properties of photocatalysts through facet modulation [13–20]. It is found that the exposure of specific crystal facets is beneficial for the formation of high-density atomic steps and unsaturated coordination sites, which can attribute to the superior photoactivity [21,22]. Especially, the spontaneous charge separation on different facets of facet semiconductors has aroused considerable interests on facet engineered photocatalysts [23,24]. However, the intrinsic relation between facet control and pollutant degradation is still an open question. Take TiO_2 as an example, intensive research draw the conclusion that high-energy {001} facets exhibit higher activity, because of the relatively higher surface energies in terms of computations [14,15]. In contrast, there

have been also discrepancies in the trends of crystal facet dependent photocatalytic activities. For example, Liu and co-workers found that photoreactivity of clean anatase facets follows the order of {001} < {101} < {010} [25]. Zhao et al. reported that anatase cuboids with dominant {100} facets exhibit 3 times higher photocatalytic activity in generating OH radicals than anatase sheets with dominant {001} facets [26]. Pradhan et al. and Zheng et al. reported that synergetic effect between low-energy {101} and high-energy {001} facets resulted in significantly enhanced photocatalysis [27,28]. Clarifying the effect of inherent characteristics of facet semiconductors on the photocatalytic reactions is a challenging research topic, although it has immense scientific and technological values for the design of more efficient photocatalysts.

Based on recent results, several factors show significant influence on the interfacial reactions over facet photocatalysts, such as surface reconstruction, dipolar field and surface states, while the anisotropic molecule adsorption further complicates the actual results. Indeed, it was found the interaction between the reactants and TiO$_2$ nanosheets affected both the separation efficiency of the photogenerated charge carriers and band gap of TiO$_2$ [29]. Unfortunately, most research mainly focused on the controllable synthesis of facets photocatalysts, thereafter the influence of exposure percentage of facet semiconductors on the photoreactivities. The intrinsic relation between interfacial structures and micromechanism is seriously neglected [29]. It is a critical point to deliberate the significant impact of electronic structures on the formation of reactive radicals and the diversification of reaction intermediates, which is extremely important for improving the efficiency of TiO$_2$ through crystal-facet tailoring.

In this study, anthracene, one of the priority PAHs, was selected as the model pollutant to investigate the contribution of crystal facet engineering on the photodegradation pathways. The different photodegradation mechanism of anthracene over three dominant facets of TiO$_2$ (001, 010 and 101) was firstly determined by studying the formation of intermediates and reactive radicals. The influence of surface structures on the removal efficiency was evaluated. We hope this study could provide new insight into the design of high-efficiency TiO$_2$-based facet photocatalysts, for the degradation of typical hydrophobic pollutants.

2. Experimental

2.1. Synthesis and characterization

TiO$_2$ nanoparticles with {001}, {010}, and {101} dominant facets were prepared through a hydrothermal method reported by Li et al. [30]. In a typical experiment, {001}-TiO$_2$ was synthesized using titanium butoxide and hydrofluoric acid solution at 200 °C for 24 h. Fluorine ions was removed by soaking the products in 0.1 M NaOH solution. {010}-TiO$_2$ was prepared by dissolving commercial anatase TiO$_2$ powder (Alfa Aesar, 325 mesh, 99.6%) in 10 M NaOH solution and hydrothermally treated at 180 °C for 24 h. After filtration, washing and hydrochloric acid treatment, H$_2$TiO$_3$ nanotubes were converted into {010}-TiO$_2$ through another hydrothermal reaction at 170 °C. Two-step hydrothermal reactions were used to fabricate {101}-TiO$_2$. P25 TiO$_2$ was first hydrothermally treated with 17 M KOH at 110 °C for 20 h. The resulting powders were further hydrothermally treated with ultrapure water at 170 °C for 24 h.

The crystal structures of prepared TiO$_2$ were confirmed by an X-ray diffractometer (XRD, X'Pert PRO MPD, PANalytical, Netherland). The morphology of particles was examined by high resolution transmission electron microscopy (HRTEM, JEM-2100F, Hitachi, Japan). The optical absorption spectra of {001}, {010}, and {101}-TiO$_2$ were obtained by using ultraviolet-visible diffuse reflection

spectrophotometer (UV-vis DRS, Cary 5000, Varian, USA). The Mott-schottky measurements were carried out using an electrochemical station (Interface 1000, Gamry, USA). Brunauer-Emmett-Teller (BET) surface areas were measured using nitrogen adsorption-desorption isotherm measurements at 77 K (ASAP2020HD88, Micromeritics, USA).

2.2. Photodegradation experiments

Preadsorption of anthracene onto TiO$_2$ particles was carried out as Wen's reported method [11] with little modification. TiO$_2$ particles (20 mg) were added into acetone and then ultrasonic dispersed for 10 min. Anthracene was added into the TiO$_2$ emulsion, then solvent was volatilized completely under the magnetically stir at room temperature. According to the amount of anthracene and TiO$_2$ added, the surface coverage (mol/g) could be calculated. After the completely volatilization of solvent, 200 mL ultrapure water was added into the anthracene/TiO$_2$ suspension and ultrasonicated for 1 min. Then the suspension was magnetically stirred for 1 h in the dark to establish the adsorption/desorption equilibrium. A 500 W xenon lamp was used to irradiate the suspension with the irradiation intensity of 100 mW/cm^2. The spectrum of the light source was shown in Fig. S1. At selected irradiation time intervals, 5 mL of liquids were taken out and extracted with methylene dichloride for three times. The extract of each sample was concentrated, solvent-exchanged, and concentrated to 1 mL under a gentle stream of nitrogen. The internal standard (2-fluorobiphenyl) was added to the samples prior to instrumental analysis. All the photodegradation experiments were repeated at least two times.

2.3. Instrument analysis

Anthracene and the intermediate products formed during the photooxidation processes were analyzed by gas chromatography/mass spectrometer (GC–MS, Agilent 6890 GC with 5895C mass selective detector). A DB-17MS fused silica capillary column (30 m length × 0.25 mm diameter × 0.25 μm film thickness) was used for the separation of each compound. Samples (1 μL) were injected in splitless mode. The carrier gas was helium at a rate of 1 mL/min. Injector and detector temperatures were both kept at 300 °C. The program procedure was as follows: 80 °C (held for 1 min), to 120 °C at a rate of 20 °C/min, and to 290 °C at 10 °C/min (held for 10 min). Further information about compound identification and quantification were described in Text S1.

The active radicals formed during the photodegradation processes were detected by a Bruker electro-spin resonance Spectrometer (ESR, A300-10/12, Bruker, German) with 5,5-dimethyl-1-pyrroline N-oxide (DMPO) as trapping reagent.

3. Results and discussion

3.1. Materials characterization

All of the XRD diffraction peaks in Fig. S2 can be well-indexed to anatase phase TiO$_2$, which confirmed the quality and purity of the prepared TiO$_2$. Representative HRTEM and SEM images of faceted TiO$_2$ nanocrystals in Figs. 1 and S3 show the octahedral, belt-like, and plate-like morphologies of the {101}, {010}, and {001}-TiO$_2$. The BET surface areas for {001}, {010} and {101}-TiO$_2$ were 10.3, 2.1, and 5.5 m^2/g, respectively. The sizes of all nanocrystals are between 50 and 100 nm according to HRTEM images (Fig. 1). The crystal size of the TiO$_2$ were also calculated with Scherrer Equation from XRD to be 68, 52, and 102 nm for {101}, {010}, and {001}-TiO$_2$, respectively (Table S1). In this case, mass transfer limitation could be speculated to be absence in this study [31].
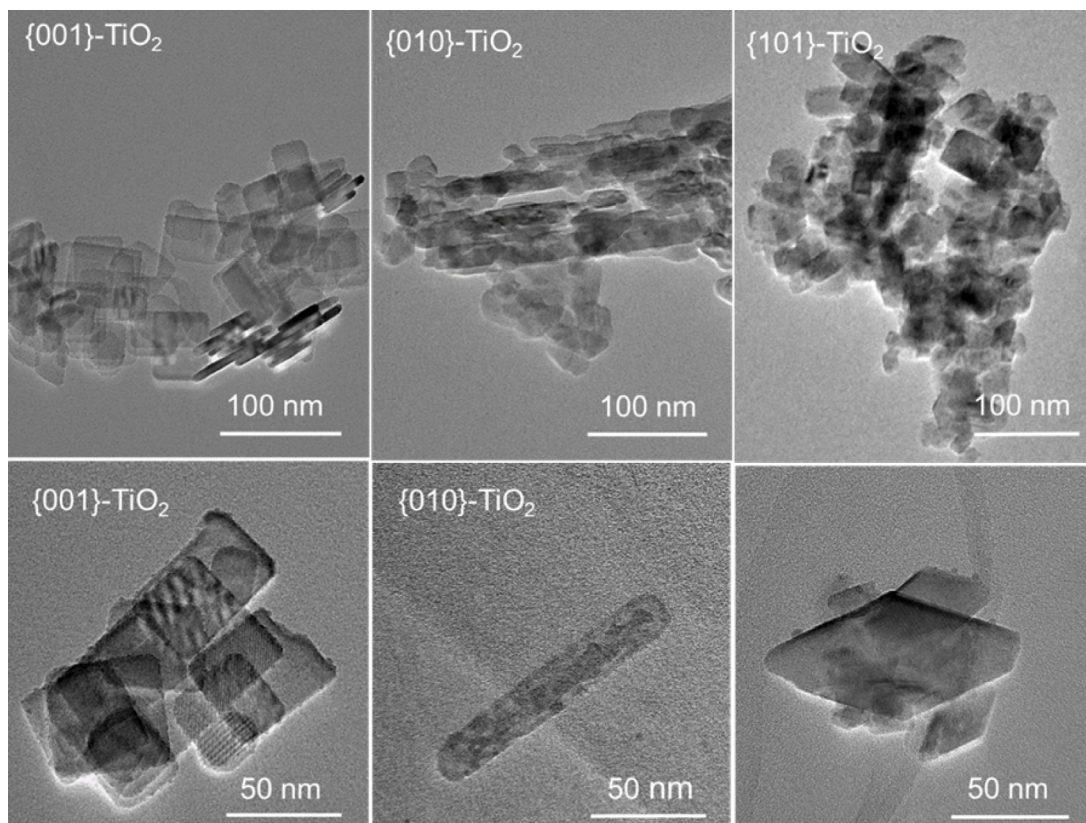
Fig. 1. HRTEM images of {001}, {010}, {101} faceted TiO$_2$ synthesized in the study.

Electronic band structures of the three types of faceted TiO$_2$ nanoparticles, which is one of the determining factors on the photoreactivity, were investigated. According to the UV–vis DRS spectra (Fig. 2a), as-synthesized {001}, {010}, and {101}-TiO$_2$ exhibits similar bandgaps, only a small difference (0.05 eV) is detected between {001} and the other two samples, resulted in the following order: {101} (3.3 eV) ≈ {010} (3.3 eV) > {001}-TiO$_2$ (3.25 eV) [25]. Mott-Schottky measurements were used to
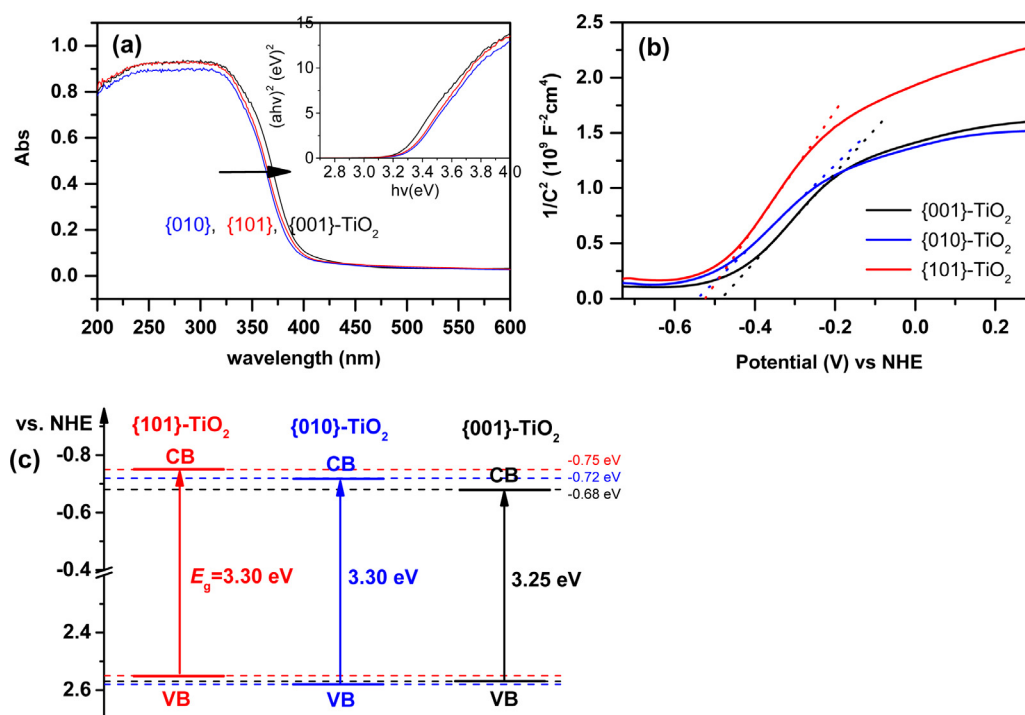

Fig. 2. UV–vis diffuse reflectance spectra (a) and plots of $(ah\nu)^{1/2}$ versus photo energy ($h\nu$) of TiO$_2$ (the inset figure), Mott-schottky curves (b), and determined conduction bands and valance bands (c) of {001}, {010}, {101} faceted TiO$_2$.
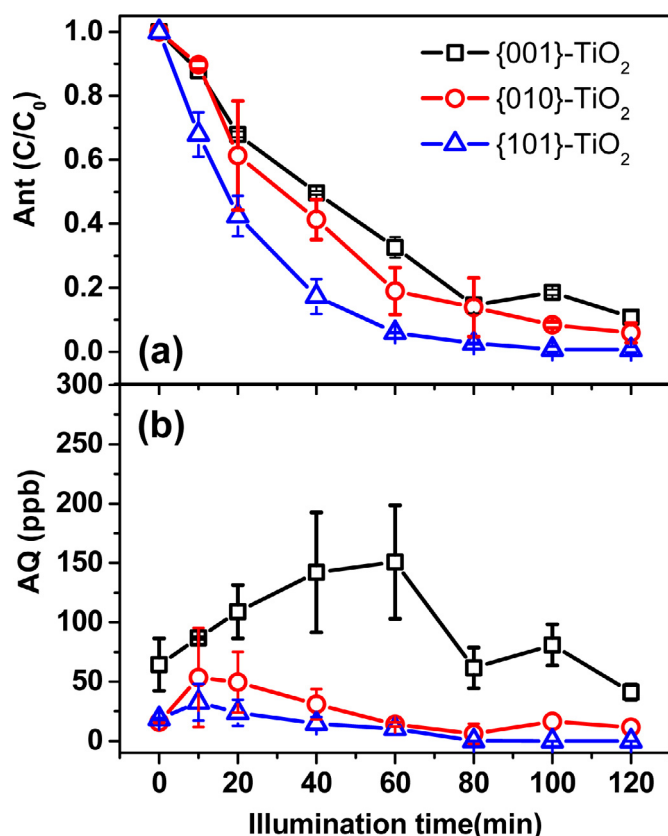
Fig. 3. Variation of relative Ant concentration (a) and evolution of AQ concentration (b) vs time ($C_{0,Ant}$ = 0.5 mg/L, solar intensity = 100 mW/cm^2).

determine the conduction band edge potentials of the three faceted TiO$_2$ (Fig. 2b). The flat-band potentials of {001}, {010} and {101}-TiO$_2$ were calculated to be −0.48, −0.55, −0.52, respectively. As a typical n-type semiconductor, presumably the bottom of conduction band of TiO$_2$ is located at 0.2 eV more negative than the flat band potential [32]. Based on the results of DRS and Mott-Schottky results, the band diagram of TiO$_2$ with different dominated facets is displayed in Fig. 2(c). {010} and {101} faceted TiO$_2$ synthesized in this study exhibits higher conduction band, indicating more strongly reductive electrons can be generated on these facets with higher flat-band potential, which means that these facets have higher conductivity band minimum. Accordingly, it is reasonably believed that holes in {010} and {001}-TiO$_2$ should possess stronger oxidation ability.

3.2. Photochemical activity

Concentration changes of Ant preadsorbed on TiO$_2$ during the photodegradation are illustrated in Fig. 3a. The compound exhibited rapid degradation rates on all the three faceted TiO$_2$, with the performance order of {101} > {010} ≈ {001}-TiO$_2$. Considering the BET surface area (10.3, 2.1, and 5.5 m^2/g for {001}, {010} and {101}-TiO$_2$, respectively), the normalized photodegradation reaction rate by surface area of {001}-TiO$_2$ would be further lower than {010} and {101}-TiO$_2$. The trend of catalytic activities herein is obviously different from those reported in previous studies, as {001} faceted TiO$_2$ are usually considered as superior candidates for photocatalytic applications [30,33,34]. For example, Li et al. reported {001}-TiO$_2$ exhibits 1.79 and 3.22 times higher activities than {010}- and {101}-TiO$_2$, respectively [30]. It was ascribed to the high surface energy of {001} facets and relative large number of Ti^{4+} sites with five-fold coordination environments [30,35]. Luan's
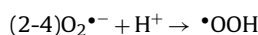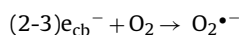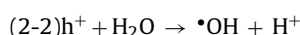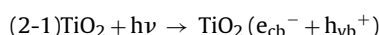
study revealed that the high photocatalytic activity of {001} faceted TiO$_2$ is mainly derived from the residual hydrogen fluoride linked to the surface of TiO$_2$ via the coordination bonds between Ti^{4+} and F$^-$ [36]. When the residual fluoride was washed off with NaOH solution, the photocatalytic activity would obviously decrease. It further confirms the complexity of photocatalytic reactions over different TiO$_2$ facets. The investigation of possible degradation pathways and intermediates is highly desirable.

During catalytic oxidation of PAHs, intermediate products will be produced, mostly be phenols, oxygenated PAHs and aldehydes [11,37]. When three faceted TiO$_2$ were used for photocatalytic degradation of Ant, anthraquinone (AQ) was found to be the dominant intermediate. This was probably because the chemical properties of Ant that the 9 and 10th carbons are most active. Additionally, oxygenated polycyclic aromatic hydrocarbons, which could be formed through transformation of PAHs in both air environment and water environment, show relatively high persistency and their concentrations in the environment may even increase as shown in our previous studies [3] and other reported study [38]. AQ is detected in all the reaction suspension and its evolution was shown in Fig. 3b. The formation and transformation of AQ over {001} facet TiO$_2$ is surprisingly different from those over {010} and {101} facets. For {001}-TiO$_2$, it could be seen that AQ concentration increased to a relatively high value (151 μg/L) at the first hour of the photodegradation process, then decreased with the irradiation time. For {010} and {101} faceted TiO$_2$, only low concentration of AQ was detected, with a slight increase in the first 10 min and then decreased slowly with the irradiation time. It must be pointed out that anthrone or anthranol, with mass/charge (m/z) ratio of 194, was also detected during the photodegradation of Ant on {001} and {010} faceted TiO$_2$, but at low concentration levels (Fig. S4). It's well known that oxygenated Ant, especially AQ, is the dominant derivative during Ant transformation [2], and usually occurred in the rivers with higher concentrations than Ant [3]. The transformation of oxygenated products indicates the possible different reaction pathways.

3.3. Mechanistic analysis

To find out the effect of crystal facet exposure on the catalytic mechanism, the photodegradation pathways of Ant over faceted TiO$_2$ crystals was studied. It should be mentioned that the direct photolysis of Ant could also contribute to the overall photodegradation, according to the Eqs. (1-1)–(1-5) described in the supporting information (Text S1). Due to the hydrophobic characteristic of Ant, the contribution of homogeneous photolysis could not be evaluated without the congestion around catalyst surface. Thus, direct photolysis was neglected in the discussion, since it was much slower than catalytic degradation.

Under irradiation, the photogenerated reactive radicals or holes usually contribute to the photodegradation of pollutant over semiconductors. In our work, Ant could possibly react with •OH and form anthrahydroquinone (2-5) [39], which then react with O$_2$•$^-$ to form anthraquione (2-6). It was also possible that the Ant was directly oxidized by photogenerated holes to form Ant cation radical (2-7), and then the cation radical react with O$_2$•$^-$ to form peroxide species, which, in turn, dissociate into anthraquione [40] (2-8).

$$(2\text{-}1)\, TiO_2 + h\nu \rightarrow TiO_2\,(e_{cb}{}^- + h_{vb}{}^+)$$

$$(2\text{-}2)\, h^+ + H_2O \rightarrow {}^\bullet OH + H^+$$

$$(2\text{-}3)\, e_{cb}{}^- + O_2 \rightarrow O_2{}^{\bullet -}$$

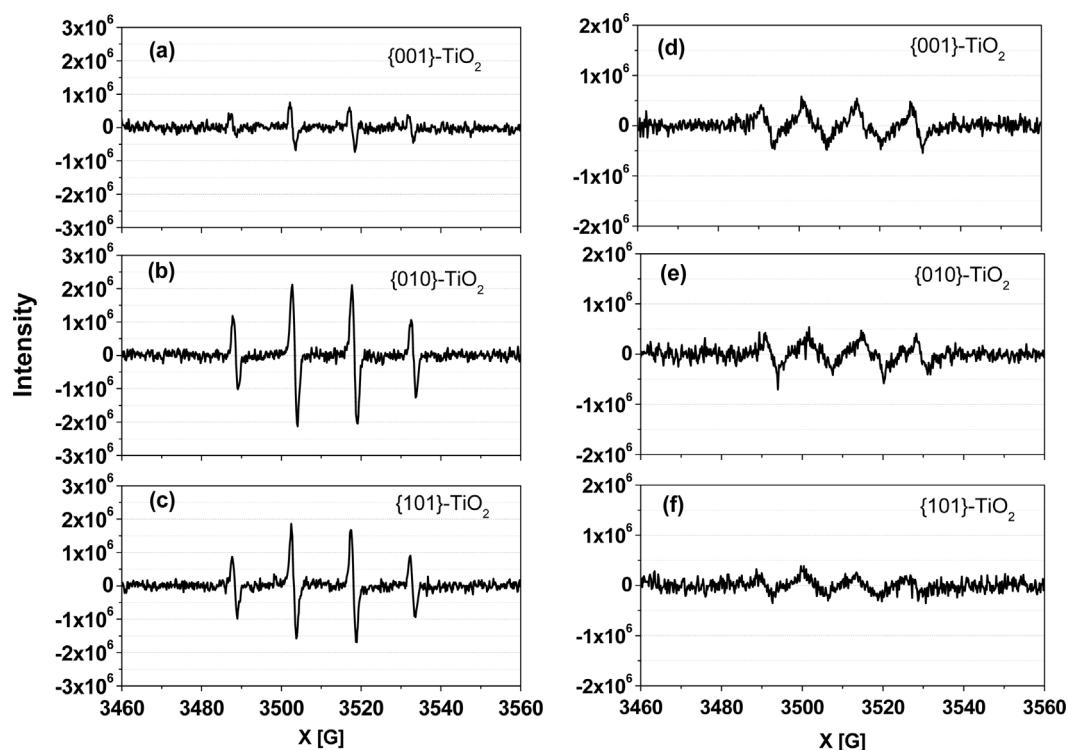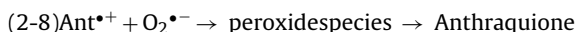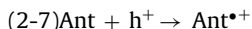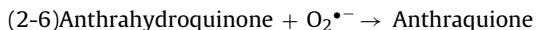$$(2\text{-}4)\, O_2{}^{\bullet -} + H^+ \rightarrow {}^\bullet OOH$$

Fig. 4. ESR spectra of *in-situ* illuminated samples of faceted TiO_2 solution in water (a–c) and in methanol (d–f).

(2-5)Ant + $^\bullet$OH → Anthrahydroquinone

(2-6)Anthrahydroquinone + $O_2^{\bullet-}$ → Anthraquione

(2-7)Ant + h^+ → Ant$^{\bullet+}$

(2-8)Ant$^{\bullet+}$ + $O_2^{\bullet-}$ → peroxidespecies → Anthraquione

To find out the possible reasons for the different order of photoreactivities of the three faceted TiO_2, the formation of radicals was examined by ESR instrument. From the ESR spectra of DMPO trapped radical species in aquatic TiO_2 suspension, four characteristic peaks of DMPO-OH (1:2:2:1) with g value of 20 were obviously observed for {010} and {101}-TiO_2 but was low for {001}-TiO_2 (Fig. 4a–c). A four paramagnetic signal (1:1:1:1) was detected for {001} and {010}-TiO_2 but was relatively weak for {101}-TiO_2 in methanol TiO_2 suspension (Fig. 4d–f). These results indicated that {010}-TiO_2 was capable to produce both $^\bullet$OH and $O_2^{\bullet-}$, {101}-TiO_2 was mainly capable to produce $^\bullet$OH, and {001}-TiO_2 was capable to produce $O_2^{\bullet-}$ and a small amount of $^\bullet$OH. It indicates that TiO_2 with different facets indeed exhibits different abilities for generating reactive species during photocatalytic reactions.

Chong et al. found that reactive oxygen species $^\bullet$OH was generated on both {001} and {101} faceted TiO_2, and the signal intensity of $^\bullet$OH was higher for {001} faceted TiO_2 than {101} faceted TiO_2 [41]. Theoretical calculations showed that the lowest energy state of the dissociated H_2O has hydroxyl bonded to a Ti_{5c} site on anatase {001} facet. However, by measuring fluorescence intensity of TAOH, Pan et al. assessed that the reactivity order of faceted TiO_2 in generating $^\bullet$OH radicals was {010} > {101} > {001} [25]. The signal intensity of photogenerated $^\bullet$OH in {101} and {010} faceted TiO_2 suspension were obviously higher than that of {001} faceted TiO_2 in our study. There are two reasons for the contradictory results in different studies. The lower VB position of {010} faceted TiO_2 than the other two faceted TiO_2 synthesized in this study were consistent with its high ability for generating $^\bullet$OH radicals. The CB of {010} and {101}-TiO_2 are negatively shifted than that of {001}-TiO_2, which eases the transfer of photo-generated electrons on {010} and {101} facets to {001} facet. The lower VB edge of {101} than other two facets facilitates the transfer of holes from the other two facets to {101} facet, and thereby photocatalytic oxidation mainly take place on {101} facet. However, the lower VB position of {001}-TiO_2 than {101}- TiO_2 was contradictory with the $^\bullet$OH generating order. It seemed that the electronic band structures only could not explain the photocatalytic reactivity of different facets. The effect from surface atomic structure or cooperative mechanism could also exist [25].

In addition, fluorine ions as inorganic capping agent were essential for the fabrication of {001} facet TiO_2. The influence of trace fluorine residuals on the surface characteristics of {001} nanoplates should also be considered. As Luan et al. recently reported that residual fluorine could possibly enhance the adsorption of O_2 so as to promote the photogenerated electrons captured by the adsorbed O_2, leading to the increased charge separation efficiency [36]. Fig. 5 shows the Ti2p and F1 s spectra of {001}-TiO_2 treated with 0.1 M

Table 1
Atom ratio of elements in {001}-TiO_2 washed with 0.1 M NaOH for different times according to XPS spectra analysis.

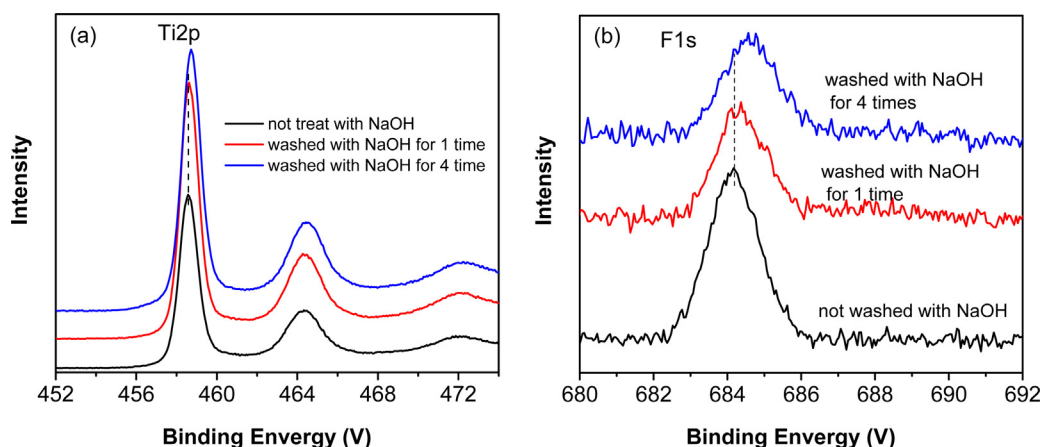| Atom Concentration(%)	Not washed with NaOH	Washed for 1 time	Washed for 4 times
Ti	27.78	27.55	27.69
O	52.89	54.92	54.66
F	5.33	2.13	2.53

Fig. 5. Ti2p (a) and F1s (b) spectra of {001}-TiO$_2$ treated with 0.1 M NaOH for different times.

NaOH with different times, and Table 1 shows the atom concentrations of elements in {001} faceted TiO$_2$ washed with NaOH for different times. Notably, the binding energy of both Ti2p and F1 s slightly increased along with NaOH washing times. Atomic content of F was 5.33% before NaOH washing and decreased to 2.13% after washing for 1 time. It seemed that the residual F in {001}-TiO$_2$ could not be removed further with 0.1 M NaOH washing more than 1 time. Another possible reason was the low contents of F in the samples made it hard to be quantified with XPS analysis. Anyway, peak of DMPO-OH was lower for the {001} faceted TiO$_2$ washed with NaOH for 4 times than the one not washed with NaOH (Fig. S5). Degradation rate of Ant on {001}-TiO$_2$ washed with NaOH for different times didn't have obvious difference (Text S3, Fig. S6), while the AQ formation on {001}-TiO$_2$ washed with NaOH for 4 times was obviously higher than the others. This indicated the residual F in {001} faceted TiO$_2$ prepared in this study was beneficial for improving •OH production. On the other hand, fluorine-modified TiO$_2$ nanosheets had weaker interaction with benzene homologues, resulting in the decreased photocatalytic activity for the sample without NaOH washing [29]. This was the possible one of the reasons for the poor photodegradation activity of {001} faceted TiO$_2$ in this study.

It is well known that the •OH radical is a highly reactive oxygen species and could oxidize compound with almost no selectivity, while O$_2$•$^-$ is an oxidant having selectivity [40]. Spin adducts of both •OH and O$_2$H• had been detected on photodecomposition of water on anatase TiO$_2$ powders [42]. In this study, the intensity of O$_2$•$^-$ generated on three faceted TiO$_2$ was rather low comparing with •OH radical. The presence of O$_2$•$^-$ spin adduct leads to speculation that molecular oxygen may be preferentially reduced on TiO$_2$ powder. The origin of the oxygen is possibly come from the presence of strongly adsorbed oxygen on the TiO$_2$ powder [41].

The production and accumulation of AQ depends on the degradation pathway of Ant in the photodegradation process. The amount of •OH radical generated during photodegradation processes maybe related with the forming rate of the intermediate AQ. The less amount of •OH radical generation from {001} faceted TiO$_2$ was corresponded with the higher AQ concentration formed during photodegradation of Ant than the other two faceted TiO$_2$.

To explain the photoreactivity performance mechanism of faceted TiO$_2$ particles further, we used t-butanol and KI to scavenge •OH and h$^+$, respectively, and added benzoquinone to scavenge electron together with Ar bubbling to degas oxygen in the solution. The results are shown in Fig. 6. For {001} faceted TiO$_2$, •OH scavenging didn't decrease the degradation rate of Ant, while O$_2$ degassing and h$^+$ scavenging did (Fig. 6a). It seemed that oxygen in the solution and holes played the key role in degrading Ant. As

direct degradation of Ant in water was inhibited by oxygen [36], we can conclude the degradation of Ant on {001} faceted TiO$_2$ was mainly from oxidation by holes or other oxidative radicals except •OH. Although •OH scavenging didn't decrease the degradation rate of Ant, the concentration of AQ increased during the process (Fig. 6b). AQ concentration increased when •OH scavenging reagent (50 mM butanol) was added during the photodegradation process (Fig. 6b). These results confirmed the former proposal that the less amount of •OH radical generation from {001} faceted TiO$_2$ was the reason for the higher AQ concentration formed during photodegradation of Ant than the other two faceted TiO$_2$. AQ concentration was rather low or was not detected when using Ar bubbling degassing oxygen and using KI scavenging holes. Ar bubbling degassed the oxygen in the solution and made the production of O$_2$•$^-$ impossible. Then the action of Eqs. (2-6) and (2-8) could not happen in the process, which inhibited the production of AQ. Holes scavenging resulted with no degradation of Ant and no production of AQ. This indicated that holes play the key roles on the first step of Ant oxidation. The production of AQ was much dependent on both the degradation of Ant and the existence of oxygen in the solution.

O$_2$ degassing and using KI scavenging holes in {010} faceted TiO$_2$ also inhibited the degradation of Ant. As we can see from Fig. 6c and d, Ant almost didn't degrade and no AQ was formed when Ar was bubbled during the photodegradation process. Similarly, when adding KI in the system, the degradation of Ant was inhibited especially in the first hour of irradiation, and was very slow in the second hour of irradiation. The formation of AQ was also similar to that in {001} faceted TiO$_2$ system. Still, •OH scavenging didn't influence the degradation of Ant but increased the concentration of AQ. These results are similar with those for {001} faceted TiO$_2$, that holes and oxygen played the key role in degrading Ant, while it was •OH that degrade the intermediate AQ further.

For {101} faceted TiO$_2$, •OH scavenging decreased the degradation of Ant slightly (Fig. 6e). This indicated that holes still play the key role in degrading Ant and •OH might play a minor role in that. O$_2$ degassing significantly inhibited the degradation of Ant, which was similar with the other two facets. Although holes scavenging inhibited the degradation of Ant to some extent, the concentration of AQ increased comparing with that when none scavenger was added (Fig. 6e, f). As shown in Fig. 6e, Ant was degraded with a much lower rate. Meanwhile, AQ concentration increased slowly during the 120 min of photodegradation period. The possible reason was the direct photolysis of Ant occurred, which caused the slow degradation of Ant and the formation of AQ under simulated solar irradiation.

To confirm the relationship between accumulation of AQ with the generation of •OH, the consumption kinetics of AQ in photo-
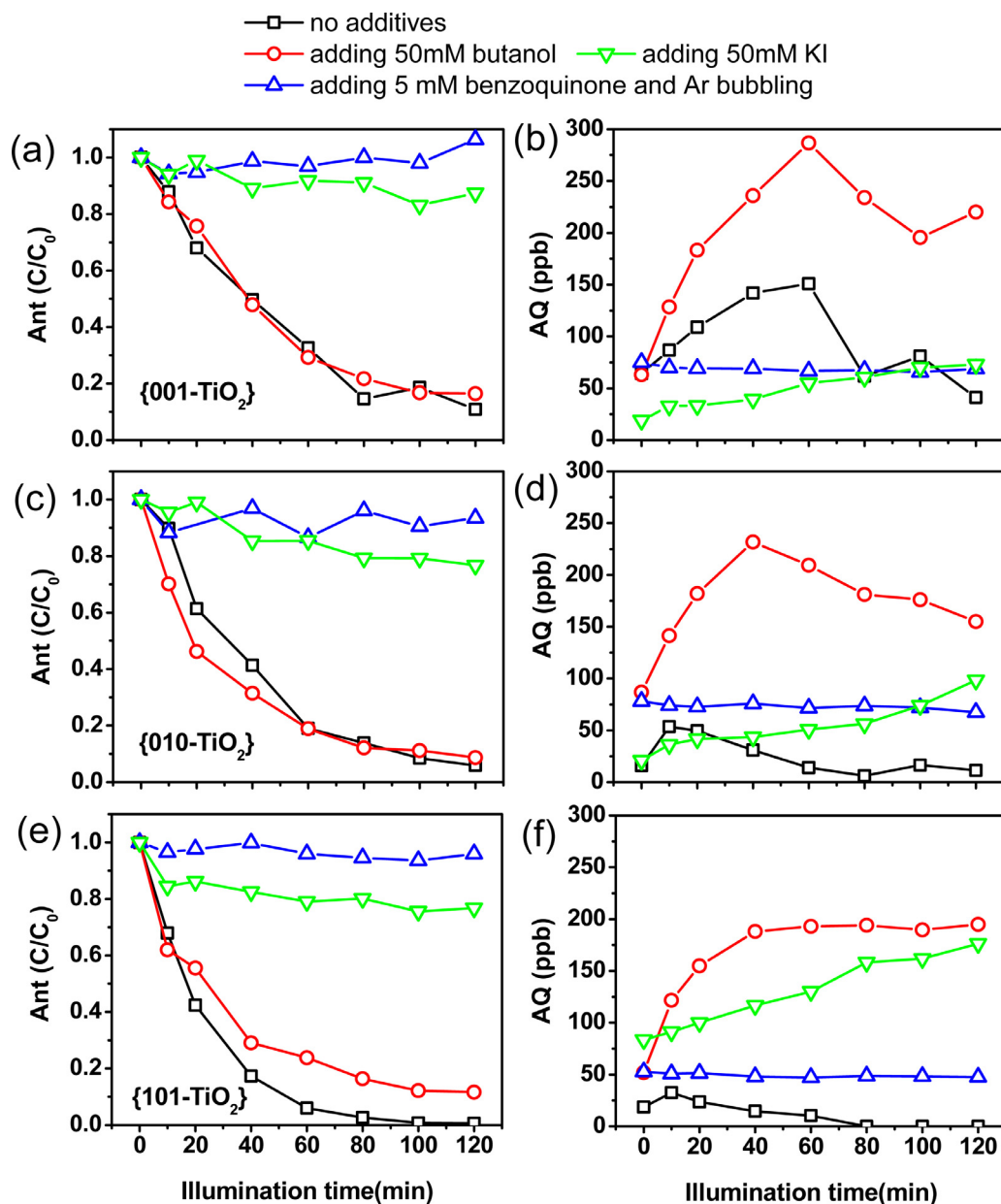
Fig. 6. Photodegradation of Ant and formation of AQ utilizing different scavengers (butanol, KI, and Arbubbling) for scanvenging •OH, h+, and degassing oxygen, respectively.

catalytic systems of {001}, {101} and {010}-TiO$_2$ were measured and compared. Concentration changes of AQ preadsorbed on TiO$_2$ during the photodegradation are illustrated in Fig. S7. AQ exhibited lower degradation rates on all the three faceted TiO$_2$ comparing with Ant (Figs. 3, S7) with the performance order of {010} > {101} > {001}-TiO$_2$. The consistent trend of catalytic activities here with the •OH generation performance (Fig. 4) of the three faceted TiO$_2$ confirmed •OH played the key role on degrading AQ. The hardly degradable properties of AQ could explain its higher concentrations in the rivers [3].

The yields of product Anthrone or Anthranol ($m/z = 194$) also increased when utilizing 50 mM butanol for scanvenging •OH during the photodegradation process, and then decreased gradually after 1 h irradiation (Fig. S6). This indicated further degradation of Anthrone or Anthranol was also dependent on the existence of active •OH.

According to the quantitative analysis and mechanistic analysis, a possible catalyzed oxidation pathway of Ant over faceted TiO$_2$ under simulated solar irradiation is illustrated in Scheme 1. The primary step is the photoinduced generation of holes and electron over TiO$_2$. The resulting holes attack Ant to produce Ant+•, as shown in Eq. (2-7). Ant+• react with O$_2$•$^-$ leading to the formation of anthrone and AQ, which is the main product of Ant photodegradation. AQ is then further destructed by •OH to yield small organic molecules or CO$_2$.

5. Conclusions

Catalytic degradation of Ant with three faceted TiO$_2$ in aquatic suspension under simulated sunlight and quantitative production of intermediate during the process was studied in this paper. {001} faceted TiO$_2$ showed lower catalytic activity than {010} and {101} faceted TiO$_2$ in the degradation of Ant. This was possibly caused by the residual fluoride in {001} faceted TiO$_2$, which resulted with less interaction of Ant with TiO$_2$. However, the intermediate anthraquione (AQ) was produced most during degradation of Ant
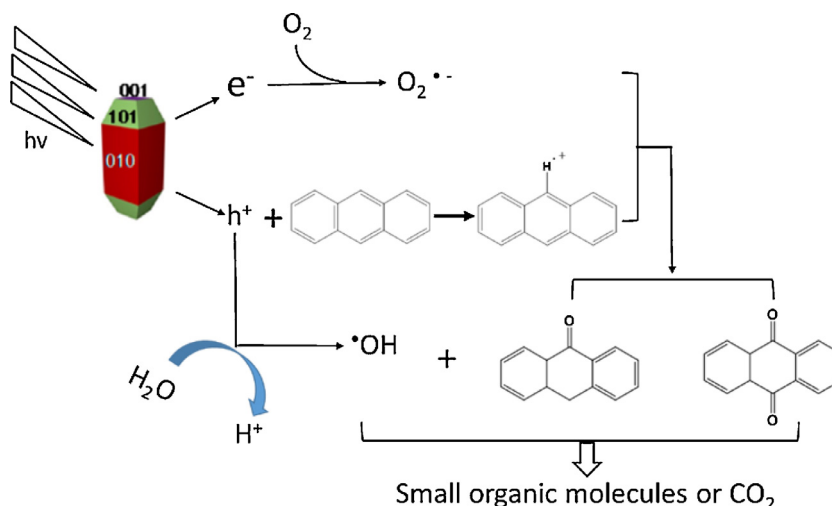
Scheme 1. Possible pathway of Ant photodegradation over faceted TiO2 under simulated solar irradiation.

on {001} faceted TiO_2, which was probably caused by the low generation of •OH radical. This was verified by the *in-situ* electron spin resonance spectroscopy measurements, which showed that {010} and {101} faceted TiO_2 could produce greater amount of •OH radical than {001} faceted TiO_2. The radical scavenging experiments showed that holes and oxygen play important roles in the first step of catalytic oxidation of Ant on {001} and {010} faceted TiO_2, while •OH radical didn't. We can conclude that the degradation of Ant was possibly due to the oxidation by holes and oxygen. The further degradation of AQ depend on the amount of •OH radical. For {101} faceted TiO_2 both holes and •OH radical play roles in the first step of Ant oxidation, which was different with the other two facets.

Acknowledgments

Appendix A. Supplementary data

Supplementary data associated with this article can be found, in the online version, at http://dx.doi.org/10.1016/j.apcatb.2017.01.018.

References

[1] W. Qi, H. Liu, B. Pernet-Coudrier, J. Qu, Polycyclic aromatic hydrocarbons in wastewater, WWTPs effluents and in the recipient waters of Beijing, China, Environ. Sci. Pollut. Res. Int. 20 (2013) 4254–4260.

[2] M. Qiao, W. Qi, H. Liu, J. Qu, Occurrence, behavior and removal of typical substituted and parent polycyclic aromatic hydrocarbons in a biological wastewater treatment plant, Water Res. 52 (2014) 11–19.

[3] M. Qiao, W. Qi, H. Liu, J. Qu, Oxygenated, nitrated, methyl and parent polycyclic aromatic hydrocarbons in rivers of Haihe River System, China: occurrence, possible formation, and source and fate in a water-shortage area, Sci. Total Environ. 481 (2014) 178–185.

[4] S. Gu, A.C. Kralovec, E.R. Christensen, R.P. Van Camp, Source apportionment of PAHs in dated sediments from the Black River, Ohio, Water Res. 37 (2003) 2149–2161.

[5] E.R. Christensen, P.A. Bzdusek, PAHs in sediments of the Black River and the AshTable River, Ohio: source apportionment by factor analysis, Water Res. 39 (2005) 511–524.

[6] J.L. Durant, W.F. Busby, A.L. Lafleur, B.W. Penman, C.L. Crespi, Human cell mutagenicity of oxygenated, nitrated and unsubstituted polycyclic aromatic hydrocarbons associated with urban aerosols, Mutat. Res. Genet. Toxicol. 371 (1996) 123–157.

[7] H. Tokiwa, Y. Ohnishi, Mutagenicity and carcinogenicity of nitroarenes and their sources in the environment, Crit. Rev. Toxicol. 17 (1986) 23–60.

[8] J.A.B. Deshan Yu, T.M. Penning, J. Field, Reactive oxygen species generated by PAH o-quinones cause change-in-function mutations in *p53*, Chem. Res. Toxicol. 15 (2002) 832–842.

[9] J. Ovrevik, V.M. Arlt, E. Oya, E. Nagy, S. Mollerup, D.H. Phillips, M. Lag, J.A. Holme, Differential effects of nitro-PAHs and amino-PAHs on cytokine and chemokine responses in human bronchial epithelial BEAS-2B cells, Toxicol. Appl. Pharmacol. 242 (2010) 270–280.

[10] M.G.P. Fernandez, A.M. Solanas, J.M. Bayona, J. Albalges, Bioassay-directed chemical analysis of genotoxic components in coastal sediments, Environ. Sci. Technol. 26 (1992) 817–829.

[11] S. Wen, J.C. Zhao, G.Y. Sheng, J.M. Fu, P.A. Peng, Photocatalytic reactions of pyrene at TiO2/water interfaces, Chemosphere 50 (2003) 111–119.

[12] N. Vela, M. Martínez-Menchón, G. Navarro, G. Pérez-Lucas, S. Navarro, Removal of polycyclic aromatic hydrocarbons (PAHs) from groundwater by heterogeneous photocatalysis under natural sunlight, J. Photochem. Photobiol. A 232 (2012) 32–40.

[13] H.G. Yang, C.H. Sun, S.Z. Qiao, J. Zou, G. Liu, S.C. Smith, H.M. Cheng, G.Q. Lu, Anatase TiO2 single crystals with a large percentage of reactive facets, Nature 453 (2008) 638–641.

[14] H.G. Yang, G. Liu, S.Z. Qiao, C.H. Sun, Y.G. Jin, S.C. Smith, J. Zou, H.M. Cheng, G.Q.M. Lu, Solvothermal synthesis and photoreactivity of anatase TiO2 nanosheets with dominant {001} facets, J. Am. Chem. Soc. 131 (2009) 4078–4083.

[15] X. Han, Q. Kuang, M. Jin, Z. Xie, L. Zheng, Synthesis of titania nanosheets with a high percentage of exposed (001) facets and related photocatalytic properties, J. Am. Chem. Soc. 131 (2009) 3152–3153.

[16] W. Jiao, L. Wang, G. Liu, G.Q. Lu, H.-M. Cheng, Hollow anatase TiO2 single crystals and mesocrystals with dominant {101} facets for improved photocatalysis activity and tuned reaction preference, ACS Catal. 2 (2012) 1854–1859.

[17] C.Z. Wen, J.Z. Zhou, H.B. Jiang, Q.H. Hu, S.Z. Qiao, H.G. Yang, Synthesis of micro-sized titanium dioxide nanosheets wholly exposed with high-energy {001} and {100} facets, Chem. Commun. (Camb.) 47 (2011) 4400–4402.

[18] C. Liu, A.Y. Zhang, D.N. Pei, H.Q. Yu, Efficient electrochemical reduction of nitrobenzene by defect-engineered tiO2-x single crystals, Environ. Sci. Technol. 50 (2016) 5234–5242.

[19] M. Liu, H.M. Li, W.J. Wang, Defective TiO2 with oxygen vacancy and nanocluster modification for efficient visible light environment remediation, Catal. Today 264 (2016) 236–242.

[20] D.N. Pei, L. Gong, A.Y. Zhang, X. Zhang, J.J. Chen, Y. Mu, H.Q. Yu, Defective titanium dioxide single crystals exposed by high-energy {001} facets for efficient oxygen reduction, Nat. Commun. 6 (2015) 10.

[21] W.J. Ong, L.L. Tan, S.P. Chai, S.T. Yong, A.R. Mohamed, Highly reactive {001} facets of TiO2-based composites: synthesis, formation mechanism and characterization, Nanoscale 6 (2014) 1946–2008.

[22] L. Sun, Z. Zhao, Y. Zhou, L. Liu, Anatase TiO2 nanocrystals with exposed {001} facets on graphene sheets via molecular grafting for enhanced photocatalytic activity, Nanoscale 4 (2012) 613–620.

[23] M.M. Maitani, K. Tanaka, D. Mochizuki, Y. Wada, Enhancement of photoexcited charge transfer by {001} facet-dominating TiO2Nanoparticles, J. Phys. Chem. Lett. 2 (2011) 2655–2659.

[24] P. Zhang, T. Tachikawa, Z.F. Bian, T. Majima, Selective photoredox activity on specific facet-dominated TiO2 mesocrystal superstructures incubated with directed nanocrystals, Appl. Catal. B 176 (2015) 678–686.

[25] J. Pan, G. Liu, G.Q. Lu, H.M. Cheng, On the true photoreactivity order of {001} {010}, and {101} facets of anatase TiO2 crystals, Angew. Chem. Int. Ed. Engl. 50 (2011) 2133–2137.

[26] X. Zhao, W. Jin, J. Cai, J. Ye, Z. Li, Y. Ma, J. Xie, L. Qi, Shape- and size-controlled synthesis of uniform anatase TiO2 nanocuboids enclosed by active {100} and {001} facets, Adv. Funct. Mater. 21 (2011) 3554–3563.

[27] Y.S.N. Roy, D. Pradhan, Synergy of low-energy {101} and high-Energy {001} TiO2 crystal facets for enhanced photocatalysis, ACS Nano 7 (2013) 2532–2540.

[28] Z. Zheng, B. Huang, J. Lu, X. Qin, X. Zhang, Y. Dai, Hierarchical TiO2 microspheres: synergetic effect of {001} and {101} facets for enhanced photocatalytic activity, Chemistry 17 (2011) 15032–15038.

[29] L. Ren, Y. Li, J. Hou, J. Bai, M. Mao, M. Zeng, X. Zhao, N. Li, The pivotal effect of the interaction between reactant and anatase TiO2 nanosheets with exposed {001} facets on photocatalysis for the photocatalytic purification of VOCs, Appl. Catal. B 181 (2016) 625–634.

[30] C. Li, C. Koenigsmann, W. Ding, B. Rudshteyn, K.R. Yang, K.P. Regan, S.J. Konezny, V.S. Batista, G.W. Brudvig, C.A. Schmuttenmaer, J.H. Kim, Facet-dependent photoelectrochemical performance of TiO2 nanostructures: an experimental and computational study, J. Am. Chem. Soc. 137 (2015) 1520–1529.

[31] M.M. Ballari, R. Brandi, O. Alfano, A. Cassano, Mass transfer limitations in photocatalytic reactors employing titanium dioxide suspensions II. External and internal particle constrains for the reaction, Chem. Eng. J. 136 (2008) 242–255.

[32] W.J. Chun, A. Ishikawa, H. Fujisawa, T. Takata, J.N. Kondo, M. Hara, M. Kawai, Y. Matsumoto, K. Domen, Conduction and valence band positions of Ta2O5 TaON, and Ta3N5 by UPS and electrochemical methods, J. Phys. Chem. B 107 (2003) 1798–1803.

[33] L. Ye, J. Mao, J. Liu, Z. Jiang, T. Peng, L. Zan, Synthesis of anatase TiO2 nanocrystals with {101}, {001} or {010} single facets of 90% level exposure and liquid-phase photocatalytic reduction and oxidation activity orders, J. Mater. Chem. A 1 (2013) 10532.

[34] Q. Wu, M. Liu, Z. Wu, Y. Li, L. Piao, Is photooxidation activity of {001} facets truly lower than that of {101} facets for anatase TiO2 crystals? J. Phys. Chem. C 116 (2012) 26800–26804.

[35] G. Liu, H.G. Yang, J. Pan, Y.Q. Yang, G.Q. Lu, H.M. Cheng, Titanium dioxide crystals with tailored facets, Chem. Rev. 114 (2014) 9559–9612.

[36] Y. Luan, L. Jing, Y. Xie, X. Sun, Y. Feng, H. Fu, Exceptional photocatalytic activity of 001-facet-exposed TiO2 mainly depending on enhanced adsorbed oxygen by residual hydrogen fluoride, ACS Catal. 3 (2013) 1378–1385.

[37] J.S. Miller, D. Olejnik, Photolysis of polycyclic aromatic hydrocarbons in water, Water Res. 35 (2001) 233–243.

[38] S. Lundstedt, P.A. White, C.L. Lemieux, K.D. Lynes, I.B. Lambert, L. Oberg, P. Haglund, M. Tysklind, Sources, fate, and toxic hazards of oxygenated polycyclic aromatic hydrocarbons (PAHs) at PAH-contaminated sites, Ambio 36 (2007) 475–485.

[39] O.T. Woo, W.K. Chung, K.H. Wong, A.T. Chow, P.K. Wong, Photocatalytic oxidation of polycyclic aromatic hydrocarbons: intermediates identification and toxicity testing, J. Hazard. Mater. 168 (2009) 1192–1199.

[40] J. Kou, Z. Li, Y. Yuan, H. Zhang, Y. Wang, Z. Zou, Visible-light-induced photocatalytic oxidation of polycyclic aromatic hydrocarbons over tantalum oxynitride photocatalysts, Environ. Sci. Technol. 43 (2009) 2919–2924.

[41] R. Chong, J. Li, X. Zhou, Y. Ma, J. Yang, L. Huang, H. Han, F. Zhang, C. Li, Selective photocatalytic conversion of glycerol to hydroxyacetaldehyde in aqueous solution on facet tuned TiO2-based catalysts, Chem. Commun. (Camb.) 50 (2014) 165–167.

[42] C.D. Jaeger, A.J. Bard, Spin trapping and electron spin resonance detection of radical intermediates in the photodecomposition of water at TiO2 particulate systems, J. Phys. Chem. 83 (1979) 3146–3152.